Recent Experiments on Near-Threshold Electron-Impact Excitation of Multiply Charged Ions

M. E. Bannister*, N. Djurić†, O. Woitke†, G. H. Dunn†, Y.-S. Chung‡, A. C. H. Smith§, and B. Wallbank‖

Physics Division, Oak Ridge National Laboratory, Oak Ridge, Tennessee 37831-6372

†*JILA, University of Colorado and National Institute of Standards and Technology, Boulder, Colorado 80309-0440*

‡*Department of Physics, Chungnam National University, Gung-Dong 220, 3005-764 Daejon, South Korea*

§*Department of Physics and Astronomy, University College London, London WC1E 6BT, United Kingdom*

‖*Department of Physics, St. Francis Xavier University, Antigonish, Nova Scotia, Canada, B2G 2W5*

Abstract. Some recent measurements of excitation of multiply charged ions by electrons studied in beam-beam experiments are highlighted. The emphasis is on absolute total cross sections measured with the merged electron-ion beams energy-loss (MEIBEL) technique, although some results obtained with the crossed-beams fluorescence method are also presented. The MEIBEL technique allows the investigation of optically-allowed and forbidden transitions with sufficient energy resolution, typically about 0.2 eV, to resolve resonance structures in the cross sections. Results from the JILA/ORNL MEIBEL experiment on dipole-allowed transitions in several ions demonstrate the success of various theoretical methods in predicting cross sections in the absence of resonances. Comparisons of R-matrix calculations and measured cross sections for spin-forbidden transitions in Mg-like Si^{2+} and Ar^{6+}, however, show that further refinements to the theory are needed in order to more accurately predict cross sections involving significant contributions from dielectronic resonances and interactions between neighboring resonances.

INTRODUCTION

Vitally important in almost all plasma environments are collisions between electrons and ions, particularly those that involve the transfer of energy. Cross sections

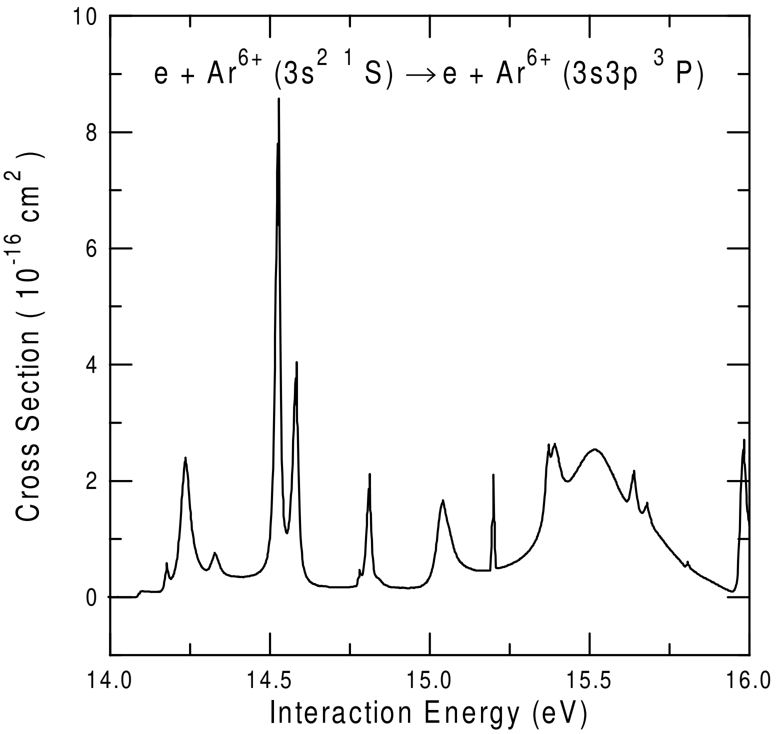

FIGURE 1. Cross sections for electron-impact excitation of the $3s^2\,{}^1S \to 3s3p\,{}^3P$ transition in Ar^{6+}. The curve represents the close-coupling R-matrix calculations of Ref. 1. The small step at the threshold (14.1 eV in the calculation of Ref. 1) is the contribution of direct excitation.

and rate coefficients for these processes are essential for modeling and diagnosing plasmas in areas of research such as controlled fusion, plasma processing, lighting discharges, and astrophysics. Theoretical efforts have produced much of the existing data, especially for electron-impact excitation of ions. Excitation can be a direct process or a result of resonant dielectronic capture followed by autoionization leaving the target ion in an excited state. Resonant enhancements to the cross section are significant in optically-forbidden transitions and can dominate the direct contribution by an order of magnitude or more near threshold, as shown in Fig. 1 for the $3s^2\,{}^1S \to 3s3p\,{}^3P$ transition in Ar^{6+} calculated [1] with the close- coupling R-matrix (CCR) method.

Direct configuration interaction (CI) and indirect interactions with a common continuum have been shown [2] to produce interference between nearby resonances and have a strong effect on the resonance contributions to the cross sections as calculated in the close-coupling formulation. It has also been found [2] that the resonance structure is sensitive to the exact energies of the individual resonances. Only in the past few years have experimentalists been able to provide theorists with benchmark cross sections for transitions dominated by resonances.

EXPERIMENTAL TECHNIQUES

Two primary beam-beam methods have been used to investigate electron-impact excitation of ions. The older method, the crossed-beams fluorescence method, is based on detecting photons emitted following excitation to a radiating state of the ion. This technique has been employed by a number of researchers [3-7] using similar experimental arrangements, but the details presented here are specific to Savin *et al.* [7]. A multiply charged ion beam is extracted from a Penning ion source, mass-to-charge ratio analyzed, and passed through an electrostatic charge purifier. The ion beam then intersects a magnetically confined electron beam at an angle of 55° (other experiments typically use 90°). After leaving the collision region, the ions are electrostatically charge analyzed, with the primary ions collected in a Faraday cup. A mirror subtending slightly over π steradians placed below the collision volume reflects emitted photons back through the collision volume and into a photomultiplier tube (PMT) oriented perpendicular to the collision plane. The bandpass of the photon detector is set by the lower-wavelength cutoff of a quartz filter and the higher-wavelength cutoff of the PMT. The total photon detection efficiency is about 1%, and the largest experimental uncertainties derive from the radiometric calibration of the photon detection system. This method must account for the angular distribution of the emitted photons over the solid angle of the detector, the polarization of the photons, and the radiative lifetime of the upper level. The two beams are modulated in a four-way chopping scheme in order to extract the signal from the background and their spatial overlap is measured with a movable beam probe.

The second method relies on detecting electrons that have lost most of their energy during inelastic collisions with ions. This merged electron-ion beams energy-loss (MEIBEL) technique has been used by researchers at the Jet Propulsion Laboratory [8] for singly charged ions and in the JILA/ORNL collaboration [9], but the details given here will be specific to the latter group. The JILA/ORNL MEIBEL technique [10], shown in Fig. 2, employs trochoidal analyzers with crossed magnetic and electric fields to merge and demerge an electron beam with an ion beam extracted from an electron-cyclotron resonance ion source. The demerger serves as an energy analyzer, separating inelastically scattered electrons from unscattered or elastically scattered electrons. Inelastically scattered electrons are deflected onto a calibrated position sensitive detector, while the unscattered primary electrons and those elastically scattered at small angles are collected in a Faraday cup since they are deflected less by the trochoidal fields. A series of apertures at the entrance of the demerger blocks electrons elastically scattered through large enough angles to reach the detector. By measuring the beam overlaps at several points along the merge path using a two-dimensional video beam probe [11], the cross sections are put on an absolute scale. The measured cross sections at higher interaction energies may be corrected for backscattering losses by using a three- dimensional trajectory modeling program [12].

The MEIBEL technique has three distinct advantages over the crossed-beams

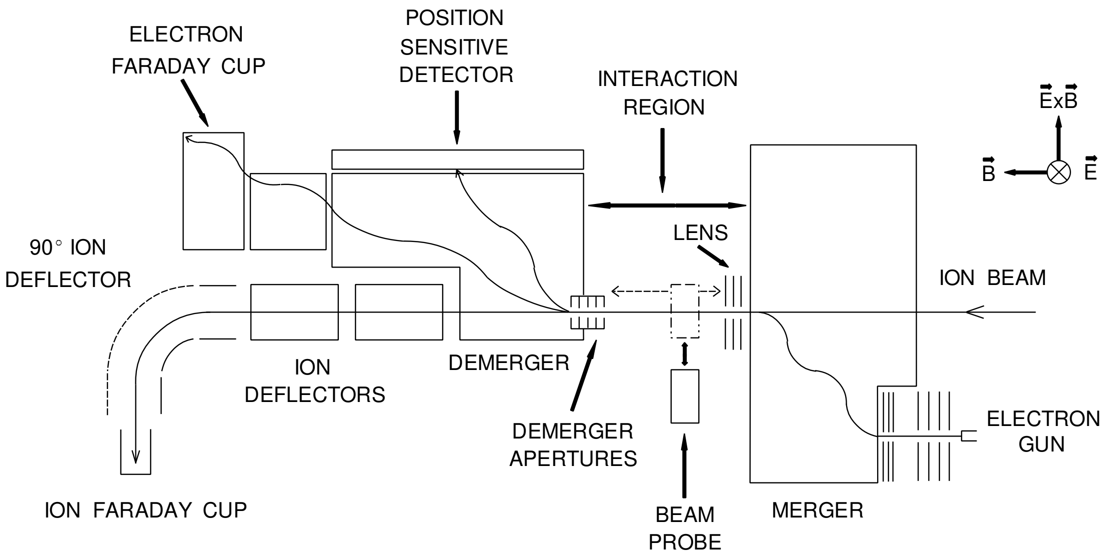

FIGURE 2. Schematic drawing of the JILA/ORNL merged electron-ion beams energy loss (MEIBEL) apparatus.

fluorescence method. Since the MEIBEL method involves the detection of low energy electrons, complete collection of the signal with detection efficiencies of 50-70% betters the capabilities of the fluorescence method by more than an order of magnitude. Secondly, by employing the merged-beams geometry, the energy resolution of the MEIBEL technique is typically 0.2 eV, which is 6-10 times better than that of the fluorescence method [7]. Finally, the fluorescence technique requires excitation to a radiating state, whereas the MEIBEL technique may be applied equally to excitation to radiating and non-radiating states.

RESULTS

The experimental results will be presented in two separate parts, one for dipole-allowed transitions measured with both the crossed-beams fluorescence and MEIBEL methods and the other for spin-forbidden transitions measured with the MEIBEL technique. The experimental data will be compared to theoretical predictions of the close-coupling R-matrix (CCR) and distorted-wave (DW) approaches.

Dipole-Allowed Transitions

The 2s $\rightarrow$ 2p transition in Li-like C^{3+} has been investigated in two different crossed-beams fluorescence experiments [7,13] as shown in Fig. 3. In addition, the transition was studied [14] with the MEIBEL technique, with the results also

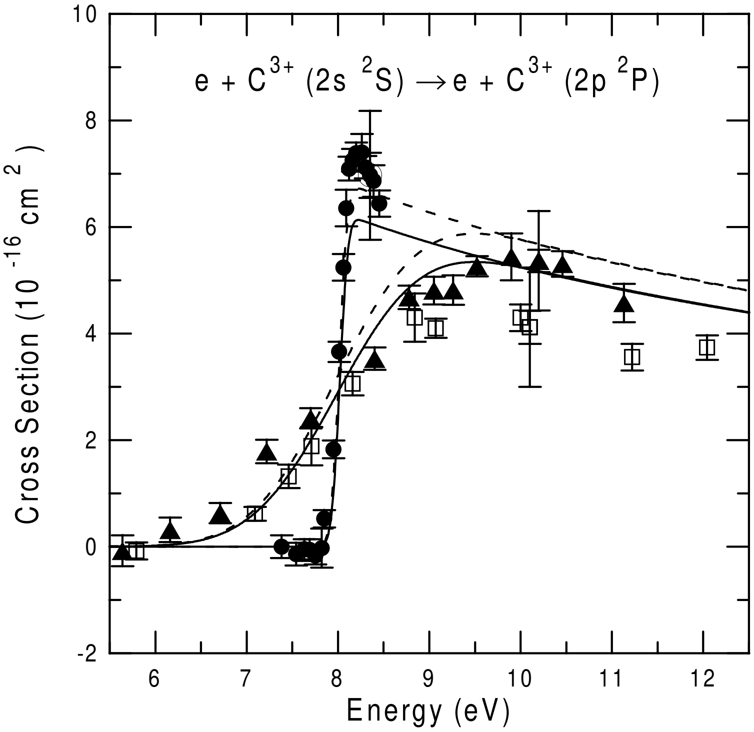

FIGURE 3. Cross sections for electron-impact excitation of the 2s → 2p transition in C^{3+}. The circles represent the MEIBEL results of Ref. 14 and the triangles and squares the crossed-beams results of Refs. 13 and 7, respectively, with relative error bars at the 90% confidence level. The outer error bars on one point in each set represent the total expanded uncertainty. The solid curves are the 9-state CCR calculations of Ref. 15 convoluted with 0.17 eV and 1.7 eV FWHM Gaussians representing the energy distributions of Refs. 14 and 7, respectively. The dashed curves are the DW results of Ref. 16 convoluted with the same two Gaussians.

shown in Fig. 3. The theoretical predictions of both Burke [15], a 9-state CCR calculation, and Clark *et al.* [16], a DW calculation, are shown convoluted with 0.17 eV and 1.7 eV FWHM Gaussians representing the energy distributions of Bannister et al. [14] and Savin *et al.* [7], respectively. There is good agreement between both calculations and the experimental data of Gregory and co-workers [13] and of Bannister *et al.* [14], but the measurements of Savin *et al.* [7] lie about 25% below the other data sets, barely within the limits of their total experimental uncertainty.

The MEIBEL technique was also used to measure cross sections [17] for excitation of the $3s^2\,{}^1S \rightarrow 3s3p\,{}^1P$ transition in Ar^{6+} as shown in Fig. 4. The 8-state CCR calculations of Griffin *et al.* [1] and the DW calculations of Clark *et al.* [16], convoluted with a 0.24 eV FWHM Gaussian representing the experimental energy distribution, are also shown in Fig. 4. There is excellent agreement between all three sets of data for this transition. The CCR theory includes some resonances

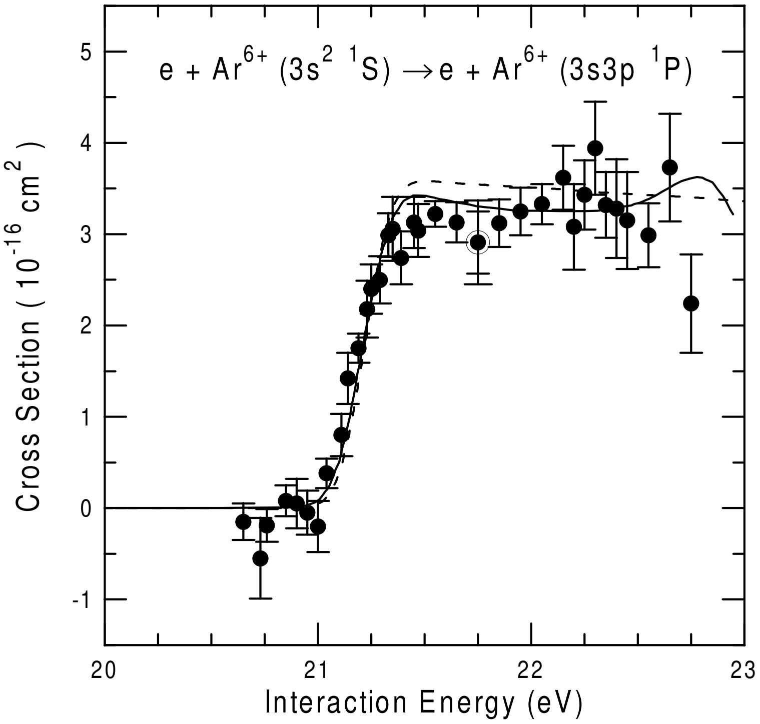

FIGURE 4. Cross sections for electron-impact excitation of the $3s^2\,{}^1S \rightarrow 3s3p\,{}^1P$ transition in Ar^{6+}. The circles are the MEIBEL results of Ref. 17 with relative error bars at the 90% confidence level. The outer bars on the point at 21.75 eV represent the total expanded uncertainty. The solid curve is the 8-state CCR calculation of Ref. 1 convoluted with a 0.24 eV FWHM Gaussian representing the experimental energy distribution. The dashed curve is the DW calculation of Ref. 16 convoluted with the same Gaussian.

near 22.7 eV, but their contributions are so small that the enhancement is only a small feature on the convoluted curve that is smaller than the relative uncertainties of the measurements. The measurement of this transition also serves to establish the absolute energy scale of the experiment, which is crucial for the measurement of the spin-forbidden transition in Ar^{6+} discussed below.

For the two dipole-allowed transitions presented above, dielectronic resonances make very minor contributions to the excitation cross section in the near-threshold region. This is not the case for the $3s^2\,{}^1S \rightarrow 3s3p\,{}^1P$ transition in Si^{2+}, as predicted by the 12-state CCR calculation of Griffin *et al.* [1]. Dielectronic resonances in this transition make significant contributions as shown in Fig. 5. There is reasonable agreement between the MEIBEL results [18] and the convoluted CCR curve about the average value of the excitation cross section, but the experimental data show a sharper drop from the peak cross section, perhaps due to a resonance just above threshold not predicted by theory. There is also disagreement about the magnitude of the resonance structure predicted near 11.7 eV. The DW results of Clark *et al.*

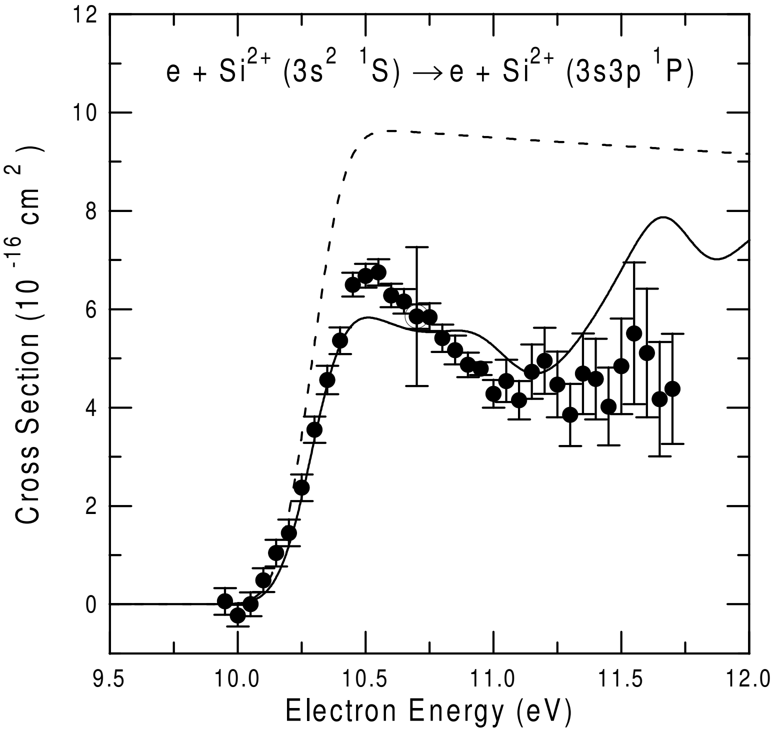

FIGURE 5. Cross sections for electron-impact excitation of the $3s^2\,{}^1S \rightarrow 3s3p\,{}^1P$ transition in Si^{2+}. The circles are the MEIBEL results of Ref. 18 with relative error bars at the 90% confidence level. The outer bars on the point at 10.7 eV represent the total expanded uncertainty. The solid curve is the 12-state CCR calculation of Ref. 1 convoluted with a 0.24 eV FWHM Gaussian representing the experimental energy distribution. The dashed curve is the DW calculation of Ref. 16 convoluted with the same Gaussian.

[16] overestimate the non-resonant cross section by a factor of nearly two and do not include any resonance contributions. The data emphasize the difficulty that *ab initio* calculations have in predicting cross sections in the presence of significant resonance contributions, even for this dipole-allowed transition. Interference between nearby resonances may account for some of the differences between the measured cross sections and those predicted by the CCR method. Ongoing measurements [19] using the crossed-beams fluorescence technique could shed more light on this discrepancy.

Spin-Forbidden Transitions

Since the non-resonant contributions are usually small for spin-forbidden transitions, the cross sections are often dominated by dielectronic resonances as discussed in the introduction. This is clearly demonstrated by the experimental excitation cross sections [18] for the $3s^2\,{}^1S \rightarrow 3s3p\,{}^3P$ transition in Si^{2+} that are shown in Fig.

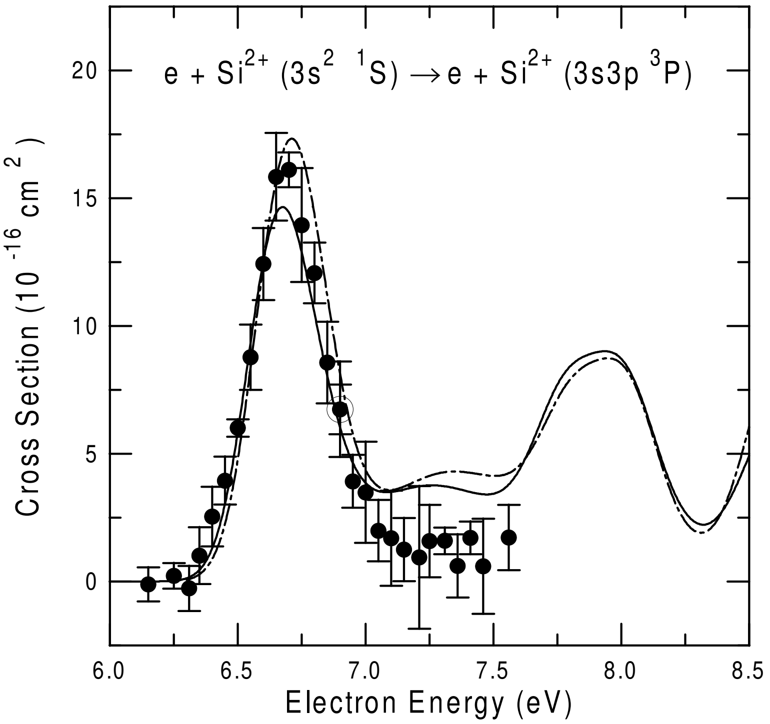

FIGURE 6. Cross sections for electron-impact excitation of the $3s^2\,{}^1S \rightarrow 3s3p\,{}^3P$ transition in Si^{2+}. The circles are the MEIBEL results of Ref. 18 with relative error bars at a 90% confidence level. The outer bars on the point at 6.9 eV represent the total expanded uncertainty. The curves are convolutions of a Gaussian (0.24 eV FWHM) with CCR calculations from Ref. 1 (solid) and Ref. 20 (dash-dot).

6 along with separate 12-state CCR calculations of Baluja *et al.* [20] and Griffin *et al.* [1], which are each convoluted with a Gaussian of 0.24 eV FWHM representing the experimental energy distribution. There is very good agreement between the three sets of data on the large resonance peak near 6.7 eV that dominates the non-resonant contributions to the cross section by almost an order of magnitude. Ion energy limitations of the experiment prevented measurements beyond 7.6 eV so that the second resonance peak predicted by theory could not be investigated.

Experimental excitation cross sections [17] for the $3s^2\,{}^1S \rightarrow 3s3p\ {}^3P$ transition in Ar^{6+} are also dominated by dielectronic resonances, as predicted by the 8-state CCR calculations of Griffin *et al.* [1] shown in Fig. 1. The measurements are shown in Fig. 7 along with the CCR calculations [1] convoluted with a Gaussian of 0.24 eV FWHM. The calculation agrees very well with the experiment for the resonance feature near 15.5 eV. The agreement for the peak near 14.4 eV is not good, indicating that the theory has difficulty calculating the precise energies of the contributing resonances and their interference. Comparison of the CCR predictions with those of the independent-processes isolated-resonance distorted-wave (IPIRDW) approx-

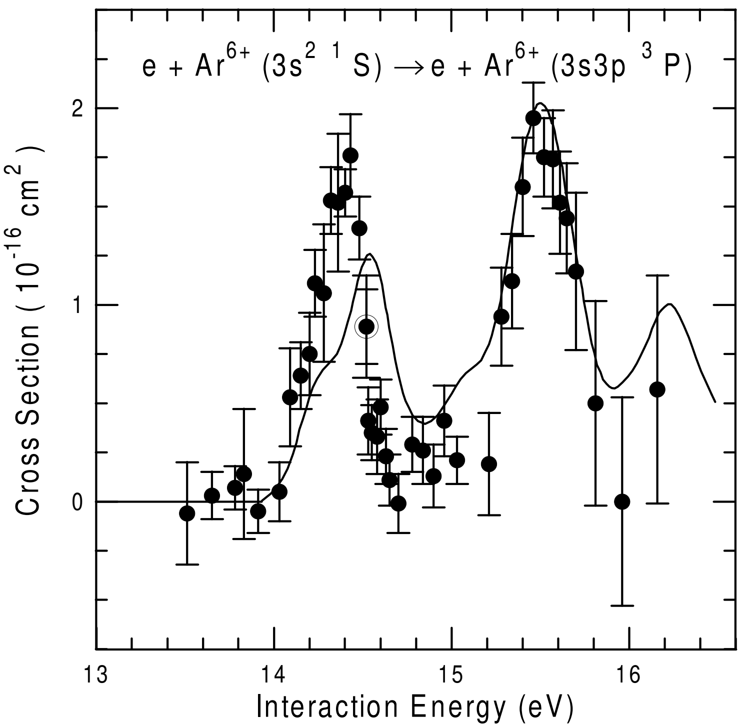

FIGURE 7. Cross sections for electron-impact excitation of the $3s^2\,{}^1S \rightarrow 3s3p\,{}^3P$ transition in Ar^{6+}. The circles are the MEIBEL results of Ref. 17 with relative error bars at a 90% confidence level. The outer bars on the point at 14.52 eV represent the total expanded uncertainty. The solid curve is a convolution of a Gaussian (0.24 eV FWHM) with CCR theory from Ref. 1.

imation [21], which neglects interactions between resonances, shows that the lower-energy peak is strongly influenced by interference effects in the CCR calculation.

CONCLUSIONS

The MEIBEL technique is a powerful tool [22] for investigating near-threshold electron-impact excitation of ions, particularly for forbidden transitions which are commonly dominated by dielectronic resonances. Both the close-coupling R-matrix (CCR) and distorted-wave (DW) methods are fairly successful in predicting cross sections for dipole-allowed transitions in the absence of significant resonance contributions. The agreement between experiment and theory is not as good when resonances dominate, and varies greatly even for different resonances in the same transition. The present experimental cross sections serve as crucial benchmarks for the close-coupling R-matrix theory and indicate that some refinements are required for the calculations to accurately reproduce the resonance positions and cross section contributions.

ACKNOWLEDGMENTS

The authors thank N. R. Badnell, T. W. Gorczyca, D. C. Griffin, M. S. Pindzola, and J. S. Shaw for providing unpublished differential and total cross section calculations. The JILA/ORNL MEIBEL research was supported by the Office of Fusion Energy Sciences of the U. S. Department of Energy, under Contract No. DE-AC05-96OR22464 with Lockheed Martin Energy Research Corp. and Contract No. DE-A105-86ER53237 with the National Institute of Standards and Technology.

REFERENCES

1. D. C. Griffin, M. S. Pindzola, and N. R. Badnell, *Phys. Rev.* A **47**, 2871-2880 (1993).
2. D. C. Griffin, M. S. Pindzola, F. Robicheaux, T. W. Gorczyca, and N. R. Badnell, *Phys. Rev. Lett.* **72**, 3491-3494 (1994).
3. D. F. Dance, M. F. A. Harrison, and A. C. H. Smith, *Proc. Roy. Soc.* A **290**, 74-93 (1966).
4. K. T. Dolder and B. Peart, *J. Phys.* B **6**, 2415-2426 (1973).
5. P. O. Taylor and G. H. Dunn, *Phys. Rev.* A **8**, 2304-2321 (1973).
6. I. P. Zapesochnyi, A. I. Dashchenko, V. I. Frontov, A. I. Imre, A. N. Gomonai, V. I. Len'del, V. T. Navrotskii, and E. P. Sabad, *JETP Lett.* **39**, 51-55 (1984).
7. D. W. Savin, L. D. Gardner, D. B. Reisenfeld, A. R. Young, and J. L. Kohl, *Phys. Rev.* A **51**, 2162-2168 (1995).
8. S. J. Smith, K.-F. Man, R. J. Mawhorter, I. D. Williams, and A. Chutjian, *Phys. Rev. Lett.* **67**, 30-33 (1991).
9. E. K. Wåhlin, J. S. Thompson, G. H. Dunn, R. A. Phaneuf, D. C. Gregory, and A. C. H. Smith, *Phys. Rev. Lett.* **66**, 157-160 (1991).
10. E. W. Bell, X. Q. Guo, J. L. Forand, K. Rinn, D. R. Swenson, J. S. Thompson, G. H. Dunn, M. E. Bannister, D. C. Gregory, R. A. Phaneuf, A. C. H. Smith, A. Müller, C. A. Timmer, E. K. Wåhlin, B. D. DePaola, and D. S. Belić, *Phys. Rev.* A **49**, 4585-4596 (1994).
11. J. L. Forand, C. A. Timmer, E. K. Wåhlin, B. D. DePaola, G. H. Dunn, D. Swenson, and K. Rinn, *Rev. Sci. Instrum.* **61**, 3372-3377 (1990).
12. SIMION 3D Version 6.0; David A. Dahl, Idaho National Engineering Laboratory.
13. D. Gregory, G. H. Dunn, R. A. Phaneuf, and D. H. Crandall, *Phys. Rev.* A **20**, 410-420 (1979); P. O. Taylor, D. Gregory, G. H. Dunn, R. A. Phaneuf, and D. H. Crandall, *Phys. Rev. Lett.* **39**, 1256-1259 (1977).
14. M. E. Bannister, Y.-S. Chung, N. Djurić, B. Wallbank, O. Woitke, S. Zhou, G. H. Dunn, and A. C. H. Smith, *Phys. Rev.* A **57**, 278-281 (1998).
15. V. M. Burke, *J. Phys.* B **25**, 4917-4928 (1992).
16. R. E. H. Clark, N. H. Magee, J. B. Mann, and A. L. Merts, *Astrophys. J.* **254**, 412-418 (1982).
17. Y.-S. Chung, N. Djurić, B. Wallbank, G. H. Dunn, M. E. Bannister, and A. C. H. Smith, *Phys. Rev.* A **55**, 2044-2049 (1997).

18. B. Wallbank, N. Djurić, O. Woitke, S. Zhou, G. H. Dunn, A. C. H. Smith, and M. E. Bannister, *Phys. Rev.* A **56**, 3714-3718 (1997).
19. D. B. Reisenfeld, P. H. Janzen, L. D. Gardner, D. W. Savin, and J. L. Kohl (private communication).
20. K. L. Baluja, P. G. Burke, and A. E. Kingston, *J. Phys* B **13**, L543-L545 (1980).
21. N. R. Badnell, D. C. Griffin, T. W. Gorczyca, and M. S. Pindzola, *Phys. Rev.* A **50**, 1231-1239 (1994).
22. Further experimental details and tabulations of the data are available at the World-Wide Web site http://www-cfadc.phy.ornl.gov/meibel/.